12 Mar 1991, 10:30 am - 12:00 pm

Cyclic Undrained Behavior of Saturated Sand Under Monotonic Loading

Hiroshi Matsuzawa
Nagoya University, Japan

Masahiro Sugimura
Nagoya University, Japan

Proceedings: Second International Conference on Recent Advances in Geotechnical Earthquake Engineering and Soil Dynamics, March 11-15, 1991, St. Louis, Missouri, Paper No. 1.56

Cyclic Undrained Behavior of Saturated Sand Under Monotonic Loading

Hiroshi Matsuzawa
Associate Professor, Department of Geotechnical Engineering, Nagoya University, Japan

Masahiro Sugimura
Research Associate, Department of Geotechnical Engineering, Nagoya University, Japan

SYNOPSIS: In order to investigate undrained behavior of saturated sand, three types of undrained triaxial tests were performed for saturated Toyoura sand, i.e., cyclic loading test with (DTU-test) and without (DU-test) constant initial shear stress and tests in which constant rate axial strain and cyclic axial stress were applied to a specimen simultaneously (DCU-test).

In DCU-tests, three types of failure were observed, i.e.; 1) perfectly liquefied in the case of relatively loose sand, 2) initially liquefied, but shear failure was induced after strength recovery for succeeding loading in the case of relatively dense sand, and 3) shear failure was induced without liquefaction.

Furthermore, constitutive equations taking account of strain history of materials were derived and applied to the above test conditions. Calculated stress-strain-pore water pressure behaviors showed good agreements with experimental results.

INTRODUCTION

Most of studies for investigation into undrained behavior of saturated sand have been paid attention to the dynamic properties of sand subjected to cyclic loading, e.g., a constant amplitude cyclic loading with or without initial shear stress, corresponding to Case-1 and 2 of Fig. 1. Dynamic properties under these loading conditions may correspond to those in soil elements A and B in Fig. 1.

However, we can consider that undrained behaviors of soil elements C and D in Fig. 1 will be different from those of soil elements A and B. During earthquakes, soil elements C and D will deform in one direction due to the lateral displacement of structures induced by inertial force on themselves and seismic earth pressure against them, while the soil will be subjected to cyclic loading. Undrained behavior of soil in the laboratory tests under the loading condition of Case-3 in Fig. 1 may correspond to those in soil element C and D. For the saturated sand under undrained condition, the static strain will induce the positive or negative excess pore water pressure in a specimen. On the

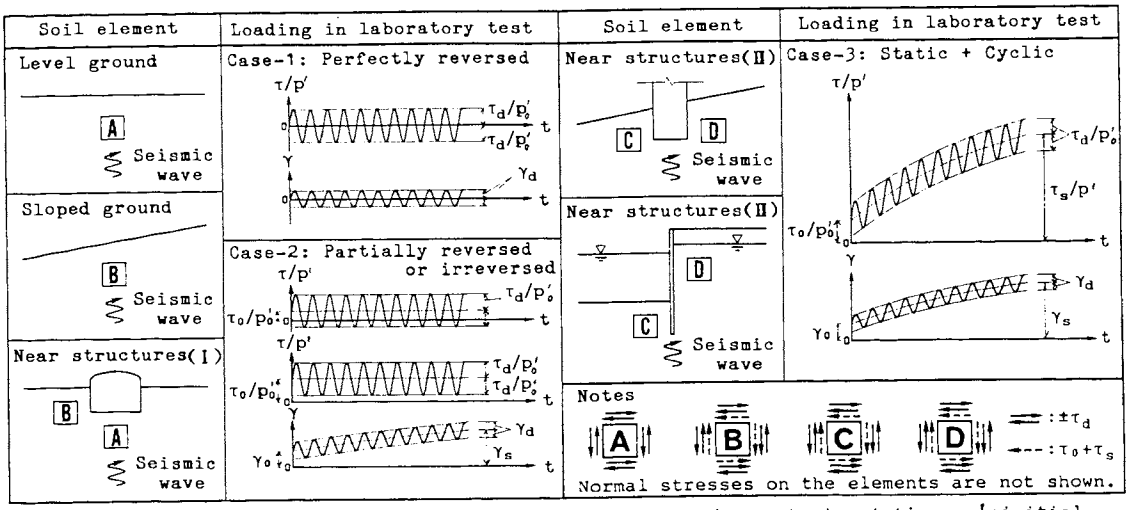

τ:shear stress, p':effective mean principal stress, γ:shear strain, t:time, p'_o:initial effective mean principal stress, τ_o:initial shear stress, τ_d:cyclic shear stress, τ_s:static component of shear stress, γ_o:initial shear strain, γ_d:cyclic shear strain and γ_s:static component of shear strain

Fig. 1 Illustrative Figure of Site Conditions and Corresponding Laboratory Tests

other hand, cyclic loading itself will build up excess pore water pressure. Under the loading condition of Case-3, these pore water pressure behaviors will progress simultaneously, and the specimen will fail with or without liquefaction.

In this study, undrained behaviors of saturated sand subjected to three types of loading, corresponding to Case-1, 2 and 3 in Fig. 1, were investigated. The authors also derived constitutive equations which can express undrained behaviors of saturated sand under these loading conditions.

STATIC AND CYCLIC LOADING TRIAXIAL TESTS

Testing Apparatus

For this study, an dynamic triaxial testing apparatus shown in Fig. 2 was developed by the authors. This apparatus can be used for static triaxial tests, for cyclic loading tests with or without constant initial shear stress and for tests in which a specimen can be subjected to a constant rate axial strain and cyclic loading simultaneously. Dimensions of a test specimen were 50mm in diameter and 125mm in height.

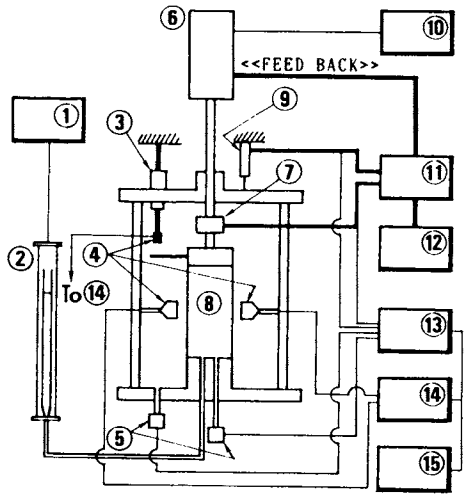

①Back pressure cell ②Burrette ③Small displacement mesuring equipment ④Uncontact displacement sensors ⑤Pressure transducer ⑥Actuator ⑦Load cell ⑧Specimen ⑨Strain gauge type displacement transducer ⑩High house pressure ⑪Axial loading pressure controller ⑫Loading rate controller ⑬Strain Amplifiers ⑭Displacement transducers ⑮Personal computer

Fig. 2 Dynamic Triaxial Testing Apparatus

Sand Used in Tests

Sand used in the tests was Toyoura sand. Physical properties and distribution of grain size of the sand are shown in Fig. 3. Void ratios in the loosest and densest state of the sand were obtained in conformity to JSF T 161-1990 standardized by The Japanese Society of Soil Mechanics and Foundation Engineering.

Test Procedure

The specimens were prepared by air-pluviating

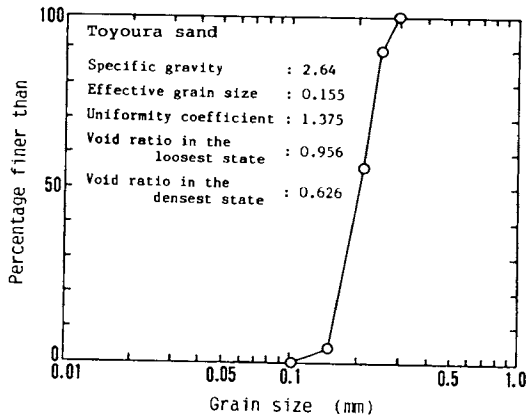

Fig. 3 Physical Properties of Toyoura Sand

the air-dried sand into a mold. Initial void ratio, e_0, of the specimen was controlled by changing the height of pluviation. In order to saturate the specimens, void of the dry specimen was filled with CO_2-gas at first. And, de-aired water was soaked into the specimen from its bottom while CO_2-gas was released through an upper platen fixed to the specimen. After then, 198kPa of back pressure was applied to the pore water. In this condition, values of Skempton's coefficient of pore water pressure, B, reached more than 0.97 for each specimen.

Then the specimens were consolidated isotropically and were submitted to following three types of undrained tests, i.e.;
DCU-test: test in which a specimen was subjected to a constant rate of compressive strain and cyclic stress simultaneously,
DU-test: cyclic loading test without initial shear stress,
DTU-test: cyclic loading test with constant initial shear stress.

In these tests, frequency of cyclic loading was 0.2Hz for loose and dense sand, and 0.1Hz for loose sand in DCU-test. The rate of static axial strain, $\dot{\varepsilon}_1$, in DCU-tests was 2.82%/min. Initial effective confining pressure, σ'_{30}, was 98kPa in all tests.

STRESS PATHS IN DCU-TEST

Figs. 4 show typical stress paths in DCU-test. Failure envelopes are also shown in these figures. We can find three types of failure in DCU-tests, i.e.;
Type-1: the specimen liquefied completely, when the initial relative density, D_r, of the specimen was less than about 60%, as shown in Fig. 4a,
Type-2: the specimen was induced partial liquefaction, but its shear strength was recovered by drop down of the excess pore water pressure due to the succeeding loading, as shown in Figs. 4b1 and 4b2. The specimen failed by shear finally. This feature was observed for the specimen of which D_r was more than about 60%. In Figs. 4b1 and 4b2, angles of shear resistance determined by failure envelopes were

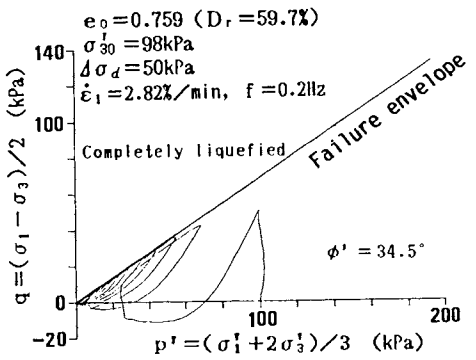

(a) Type-1

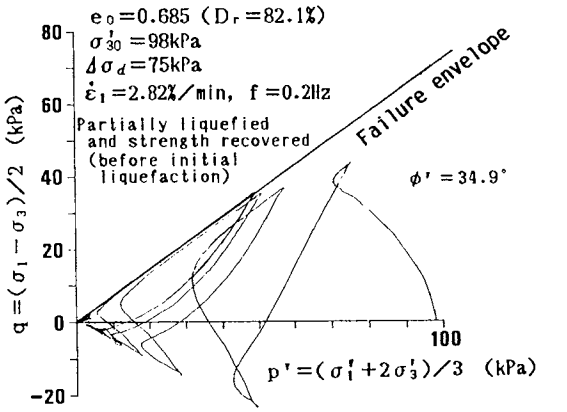

(b1) Type-2 (Before Initial Liquefaction)

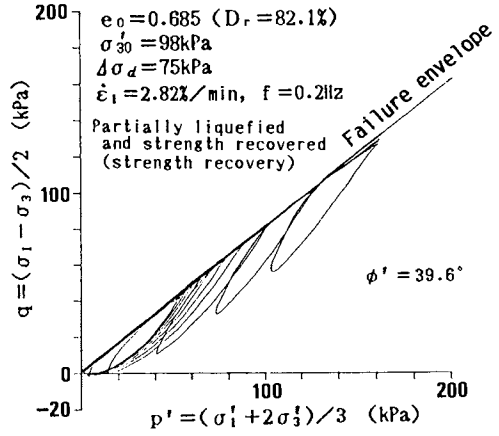

(b2) Type-2 (After Initial Liquefaction)

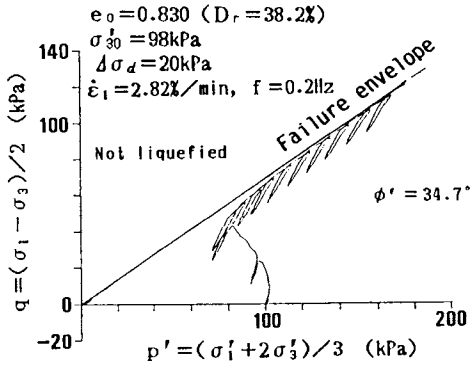

(c) Type-3

Fig. 4 Typical Stress Paths in DCU-test. Stress path of Type-2 is divided into two parts corresponding to before and after initial liquefaction, and those are shown in Figs.4b1 and 4b2 respectively.

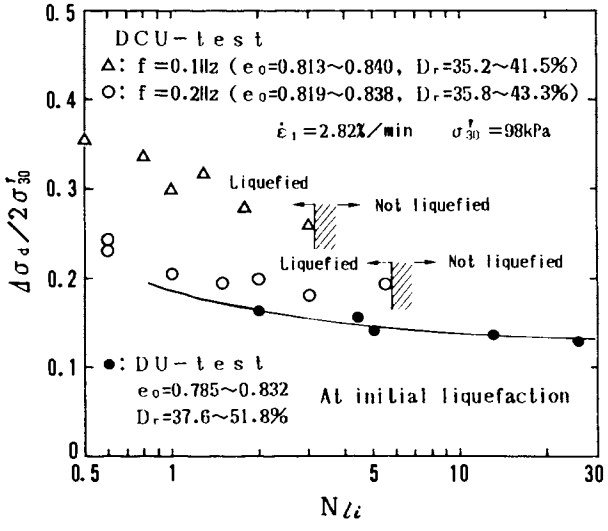

(a) Loose sand

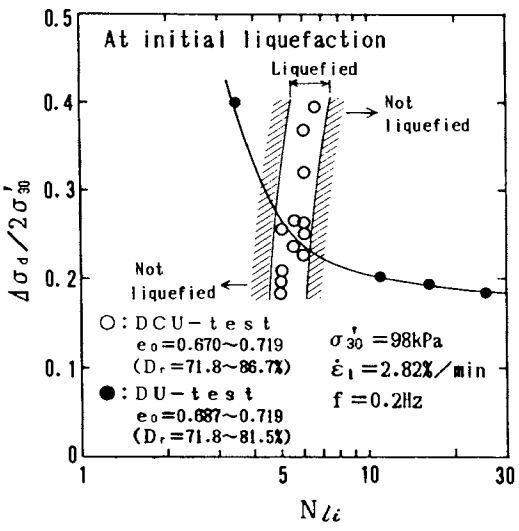

(b) Dense sand

Fig. 5 $\Delta\sigma_d/2\sigma'_{30}$ versus N_{li} in DCU-test

different before and after initial liquefaction. However, strength recovery in Type-2 will not be discussed here, because it has not made clear whether the strength recovery occurred in the specimen as an element or not.

Type-3: the specimen failed by shear without liquefaction, as shown in Fig. 4c. This feature was observed when the amplitude of cyclic stress was small and the direction of shear stress in the specimen was not reversed. The stress path shows the similar feature to those observed in undrained static compression tests.

LIQUEFACTION STRENGTH IN DCU-TEST

Fig. 5 shows relationships of liquefaction strength, $\Delta\sigma_d/2\sigma'_{30}$, against number of loading cycles at initial liquefaction, N_{li}, obtained in DU- and DCU-test, where $\Delta\sigma_d$ is the amplitude of cyclic loading axial stress. As shown in Fig. 5a, values of $\Delta\sigma_d/2\sigma'_{30}$ of loose sand in DCU-tests increase due to the effect of static strain from those in DU-tests. And the strength increments become greater as decreasing of loading frequency, f. It is remarkable that the initial liquefaction occurred at less than some number of loading cycle for each frequency. These frequency-dependency of liquefaction strength described here will be discussed in latter section.

$\Delta\sigma_d/2\sigma'_{30}$-$N_{li}$ relationship of dense sand in DCU-test was entirely different from that described above. As shown in Fig. 5b, N_{li} was increased with increase of $\Delta\sigma_d/2\sigma'_{30}$. And initial liquefaction occurred within a limited range of numbers of loading cycles, $5 \leq N_{li} \leq 7$.

All data of DCU-test were plotted in Fig. 6, regarding types of failure. In this figure, marks ○, ● and × are corresponding to Type-1, Type-2 and Type-3, respectively. And superscript numbers represent N_{li}. As shown in

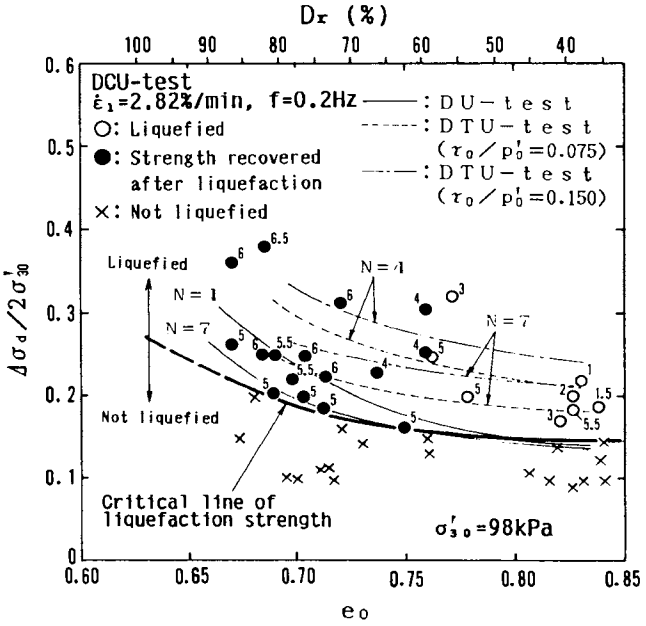

Fig. 6 Liquefaction Condition in DCU-test

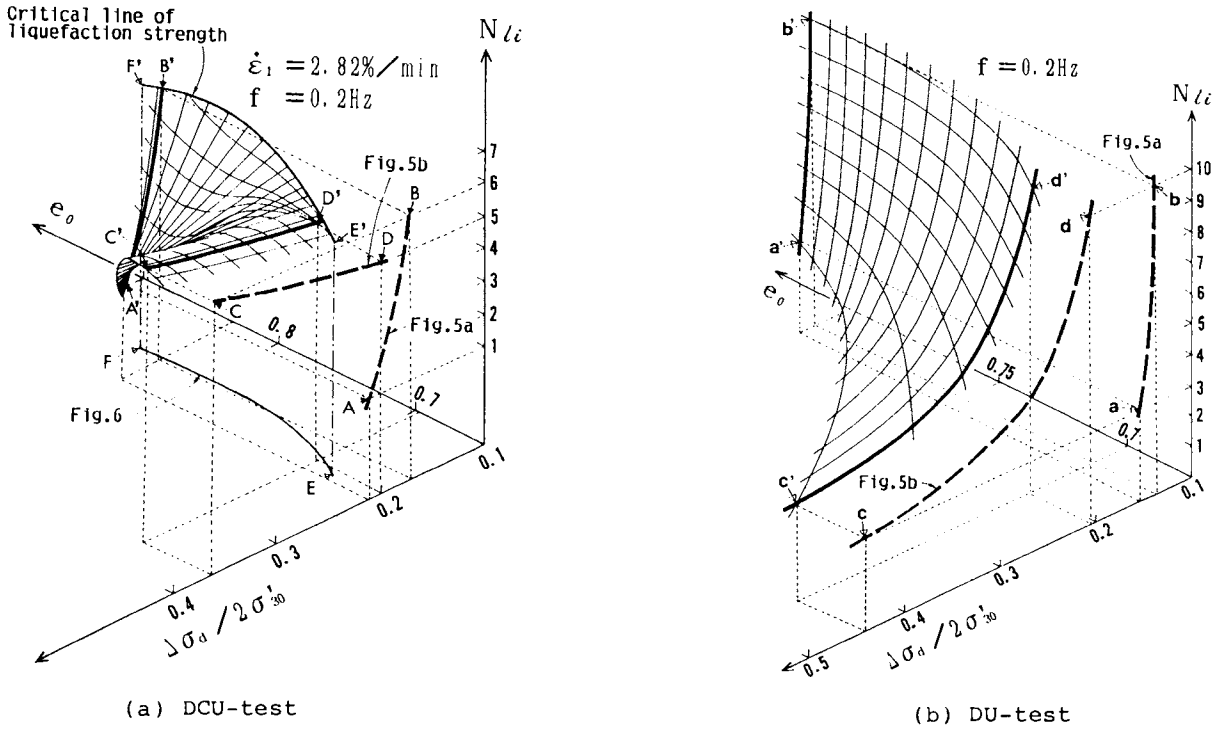

(a) DCU-test

(b) DU-test

Fig. 7 Liquefaction Strength Surface in DCU- and DU-test

Fig. 6, we can find a critical line for the liquefaction strength corresponding to $\dot{\varepsilon}_1$=2.82%/min and f=0.2Hz in DCU-test.

In Fig. 6, when the relative densities of specimens were more than 60% and initial liquefaction occurred at N=5 in DCU-test, it can be seen that liquefaction strengths are less than those in DU-test. For the other specimens, liquefaction strengths are greater than those in DU-test, and become close to those in DTU-test.

Based on the results of DCU-test, under the condition that $\dot{\varepsilon}_1$=2.82%/min and f=0.2Hz, a liquefaction strength surface was obtained in $\Delta\sigma_d/2\sigma'_{30}$-$N_{li}$-$e_0$ space as shown in Fig. 7a. The surface is twisted and the angle of twist was nearly equal to 90°. Curves A'B' and C'D' on this surface are intersections with the plains, e_0=0.83 and 0.69, respectively. And projection of these curves on $\Delta\sigma_d/2\sigma'_{30}$-$N_{li}$ plain, AB and CD, are corresponding to $\Delta\sigma_d/2\sigma'_{30}$-$N_{li}$ relationships of DCU-test in Figs. 5a and 5b, respectively. A curve E'F' is the boundary of the surface, which gives the minimum strength for generation of liquefaction. Projection of this curve on $\Delta\sigma_d/2\sigma'_{30}$-$e_0$ plain, EF, is the critical line for liquefaction strength shown in Fig. 6.

Fig. 7b shows the liquefaction strength surface in DU-test. Contrary to that of DCU-test, it can be seen that this surface spreads infinitely, and not so twisted. Projections of curves a'b' and c'd' on $\Delta\sigma_d/2\sigma'_{30}$-$N_{li}$ plain, ab and cd, correspond to $\Delta\sigma_d/2\sigma'_{30}$-$N_{li}$ relationships of DU-test in Figs. 5a and 5b respectively.

FREQUENCY-DEPENDENCY OF LIQUEFACTION STRENGTH IN DCU-TEST

In this section, frequency-dependency of liquefaction strength will be described for loose sand based on a limited number of data in DCU-test under the condition $\dot{\varepsilon}_1$=2.82%/min shown in Fig. 5a.

Liquefaction behaviors of loose sand in DCU-test were changed relating to frequency of cyclic loading as shown in Fig. 5a. From the figure, liquefaction strength on f=0.1Hz was increased from those on f=0.2Hz. The specimens were liquefied at N≦3 for f=0.1Hz and at N≦6 for f=0.2Hz.

It can be considered that the unique tendency in DCU-test, as described above, are affected considerably by dilatancy due to constant rate static strain. Fig. 8 shows static components of shear strain, γ_{su}, at initial liquefaction. For an equal number of loading cycles, γ_{su} on f=0.1Hz is twice of those on f=0.2Hz. Therefore, the effect of dilatancy due to static compression on generation of liquefaction will become remarkable as decreasing frequency of cyclic loading.

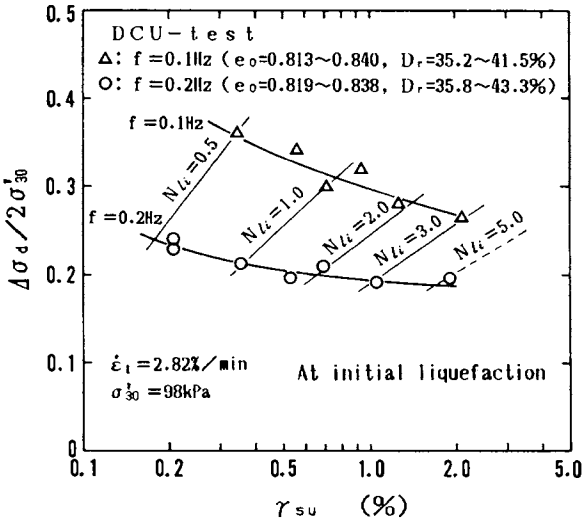

Fig. 8 Static Component of Shear Strain at Initial Liquefaction

Consequently, liquefaction strength on f=0.1Hz became greater than those on f=0.2Hz.

CONSTITUTIVE EQUATIONS

In order to express the undrained behaviors under various loading paths, the authors derived constitutive equations based on endochronic theory proposed by Valanis(1971). The concept of intrinsic time in this theory is convenient to express the cyclic behavior of materials.

Intrinsic time is corresponding to the history of deformation in materials and is own memory of the materials. Increment of intrinsic time scale, dz, is defined as follows;

$$dz=d\zeta/f(z), \quad d\zeta^2=de_{ij}^{p}\cdot de_{ij}^{p} \tag{1}$$

where de_{ij}^{p} is increment of plastic deviatric strain and f(z) is a hardening-softening function.

Deviatric stress, s_{ij}, is expressed as follows;

$$s_{ij}=2\int_0^z \mu(z-z')f(z')dz' \tag{2}$$

where 2μ(z) is a function corresponding to shear modulus.

In this paper, 2μ(z) is defined as following form;

$$2\mu(z)=G_0[\rho_0\delta(z)+\rho_1\exp(-B_1z)+\rho_2\exp(-B_2z)+\rho_3\exp\{-B_3(z-z_i)\}H(z-z_i)]$$
$$G_0=p'G(e), \quad G(e)=(2.17-e)^2/(1+e) \tag{3}$$

where G_0, ρ_0, ρ_1, B_1, ρ_2, B_2, ρ_3 and B_3 are material parameters, respectively, $\delta(z)$ is Dirac's delta function, and $H(z)$ is Heaviside's unit function. z_i is the intrinsic time scale at beginning of i-th loading-unloading step (see Fig. 9). G_0 is defined as a function of void ratio, e, and effective mean principal stress, p'. The term with ρ_3 and B_3 is corresponding to cyclic loading stage, and is omitted when unloading or reloading stages will not be exist.

Based on drained static compression tests (SCD-tests), values of $2\mu(z)/G_0$ are plotted against z in Fig. 10. In this figure, we can find an unique relationship independent with confining pressure and initial void ratio. For value of z not less than 1%, $2\mu(z)/G_0$ decreased linearly. From this unique relation, parameters ρ_1, B_1, ρ_2 and B_2 can be determined by following procedure, respectively. As shown in Fig. 10, the part of linear relation (z is not less than 1%) is approximated with a function $\rho_2\exp(-B_2z)$ in Eq.(3), and parameters ρ_2 and B_2 are determined. Using test data and the parameters ρ_2 and B_2, values of $2\mu(z)/G_0-\rho_2\exp(-B_2z)$ are replotted, shown by solid circles in Fig. 10. And approximating them with $\rho_1\exp(-B_1z)$ in Eq.(3), parameters ρ_1 and B_1 are determined.

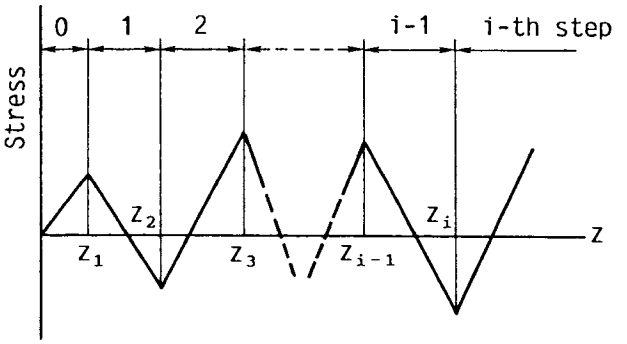

Fig. 9 Definition of z_i

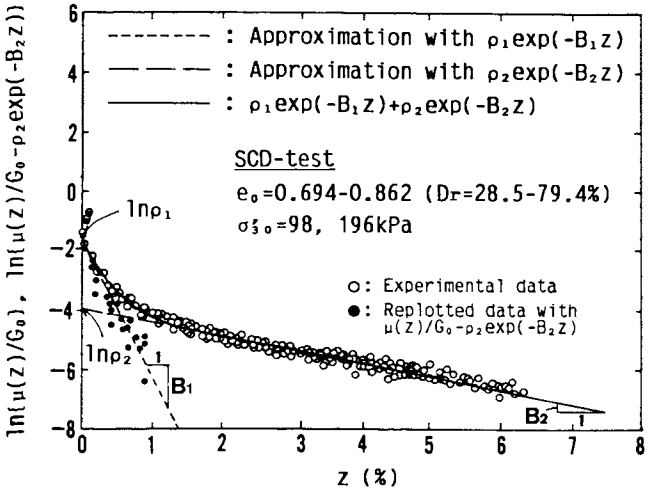

Fig. 10 Determination of Parameters ρ_1, B_1, ρ_2 and B_2

Parameters ρ_3 and B_3 are determined based on statically repeated loading test data and can be expressed by;

$$B_3=4600\zeta \ ;\text{for loose sand } (D_r\simeq 40\%)$$
$$\rho_3=\exp\{B_3z_i+\ln(\rho_1+\rho_2)\} \qquad (4)$$

Hardening-softening function, f(z), in Eq.(1) is assumed as follows;

$$f(z)=\beta+(1-\beta)\exp(-\kappa z) \qquad (5)$$

where β and κ are the material parameters regarding hardening and softening of the material. Values of f(z) is unity at z=0 (initial yielding), and will converge to β when z will become infinity.

Using Eqs.(2), (3) and (5), following equations can be obtained for axisymmetric condition;

at initial yielding (z=0):

$$(q)_{in}=\sqrt{3/2}(p')_{in}G(e)\rho_0 \qquad (6)$$

at failure state ($z=\infty$):

$$(q)_f=\sqrt{3/2}(p')_fG(e)\beta(\rho_0+\rho_1/B_1+\rho_2/B_2) \qquad (7)$$

initial tangential coefficient (z=0):

$$(dq/dz)_{in}=\sqrt{3/2}(p')_{in}G(e)\{\rho_0\kappa(\beta-1)+\rho_1+\rho_2\}$$
$$\equiv\sqrt{3/2}\mu(0)=\sqrt{3/2}(p')_{in}G(e)(\rho_0+\rho_1+\rho_2) \qquad (8)$$

where $q=(\sigma_1-\sigma_3)/2$, $p'=(\sigma_1+2\sigma_3)/3$. Parameters ρ_0, β and κ can be determined by using Eqs.(6)-(8).

Moroto(1976) proposed a parameter that express deformation properties of granular soil. The parameter, S_s, is defined under drained condition by plastic work normalized by mean principal stress, p, as follows;

$$dS_s=dW^p/p \qquad (9)$$

where dW^p is increment of plastic work done due to shear, and plastic volumetric strain due to shear, ε_v^p, will be expressed by following equations;

$$d\varepsilon_v^p=\sqrt{2}/3\{\lambda-\sqrt{8}(q/p)\}d\gamma^p$$
$$\lambda=dS_s/d\gamma^p \qquad (10)$$

where γ^p is plastic shear strain.

Based on results of drained and undrained static compression tests, following relationship could be pointed out between increment of volumetric strain, ε_v, in drained tests and effective mean principal stress, p', in undrained tests;

$$d\varepsilon_v=A(dp'/p')=A(dp-du)/p' \qquad (11)$$

where A is a material parameter. Using Eqs. (10) and (11), pore water pressure change in undrained condition can be expressed by following equation;

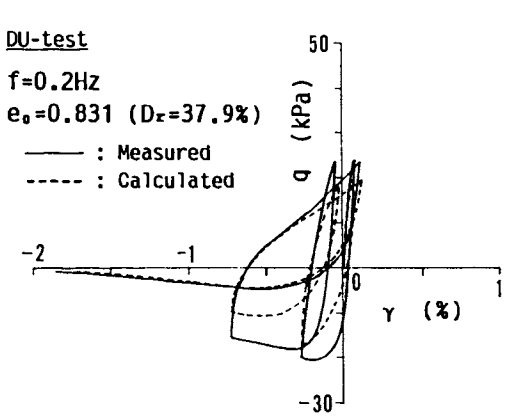

(a) q-γ Relationship

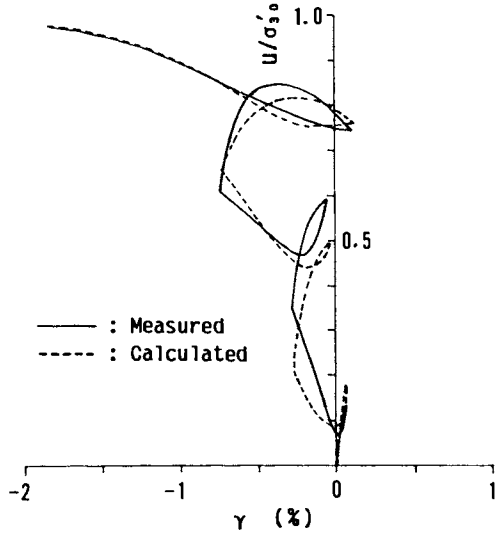

(b) u/σ'_{30}-γ Relationship

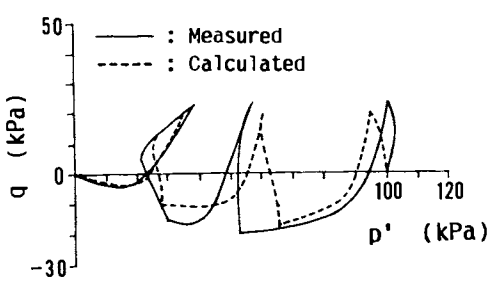

(c) Effective Stress Path

Fig. 11 Prediction of Behaviors in DU-test by Proposed Equations

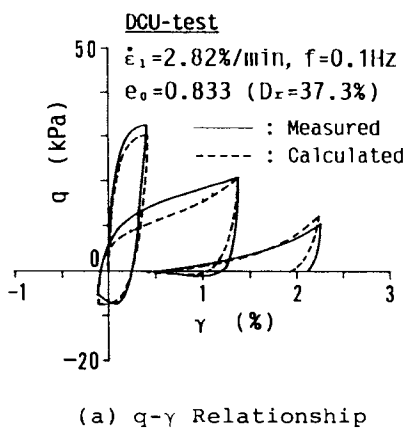

(a) q-γ Relationship

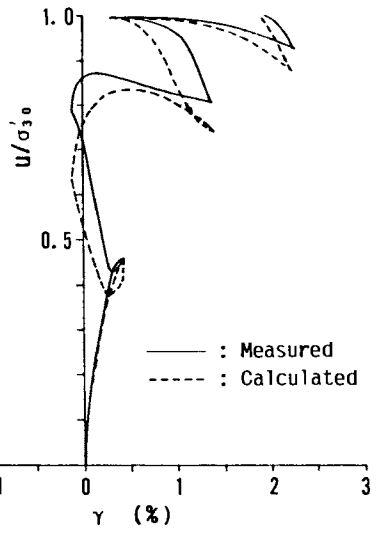

(b) u/σ'_{30}-γ Relationship

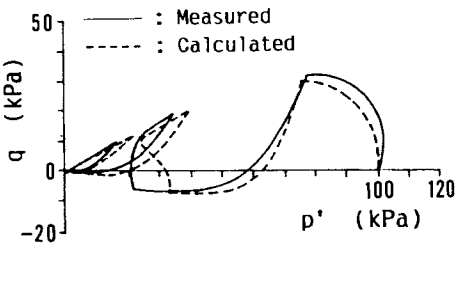

(c) Effective Stress Path

Fig. 12 Prediction of Behaviors in DCU-test by Proposed Equations (f=0.1Hz)

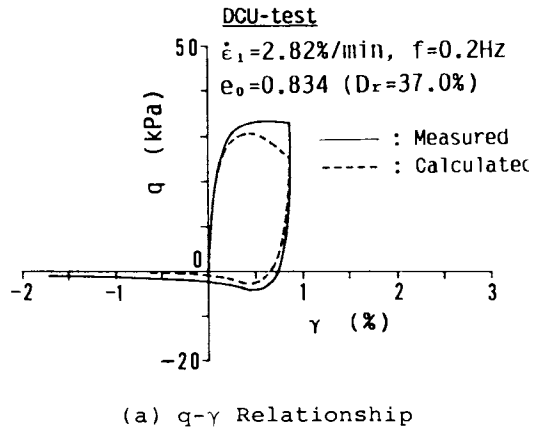

(a) q-γ Relationship

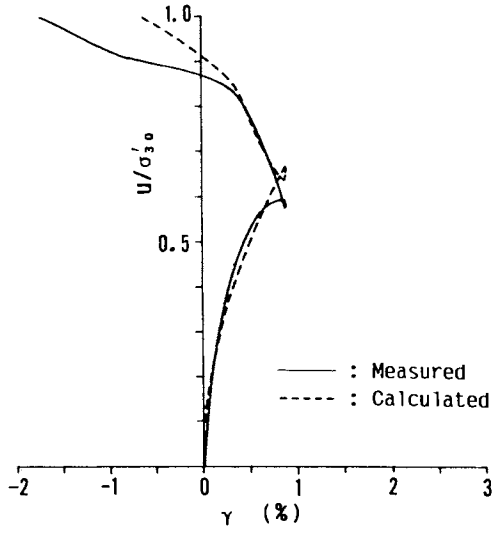

(b) u/σ'_{30}-γ Relationship

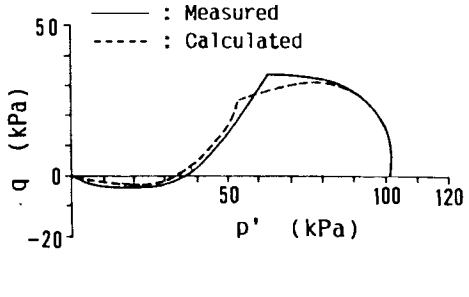

(c) Effective Stress Path

Fig. 13 Prediction of Behaviors in DCU-test by Proposed Equations (f=0.2Hz)

$$du=dp-(\sqrt{2}/3)(p'/A)\{\lambda-\sqrt{8}(q/p')\}d\gamma^p \qquad (12)$$

The material parameter A has different values corresponding to shear stress level, i.e.;

$$A=A_c \quad \text{for } q/p' \leqq \sqrt{8}\lambda$$
$$A=A_d \quad \text{for } q/p' > \sqrt{8}\lambda \qquad (13)$$

where $\sqrt{8}\lambda$ is corresponding to stress ratio at phase transformation.

APPLICATION OF CONSTITUTIVE EQUATIONS TO DU- AND DCU-TEST

The constitutive equations in the previous section were applied to DU- and DCU-tests for loose sand. Inputting the observed shear strain in a test to the equations, shear stress and excess pore water pressure, u, can be predicted.

Figs. 11, 12 and 13 show the results of calculation for typical test results. We can find that the calculated values show good agreement with test results, respectively.

The predicted liquefaction strengths of loose sand in DU- and DCU-test are shown by dotted lines in Fig. 14. In these calculations, a judgment of liquefaction was done at $p'=0.01p'_{in}$, where p'_{in} is initial effective mean principal stress. The proposed constitutive equations expressed well frequency-dependency of liquefaction strengths observed in DCU-test.

Though undrained behaviors of dense sand are not shown here, the proposed constitutive equations gives good prediction.

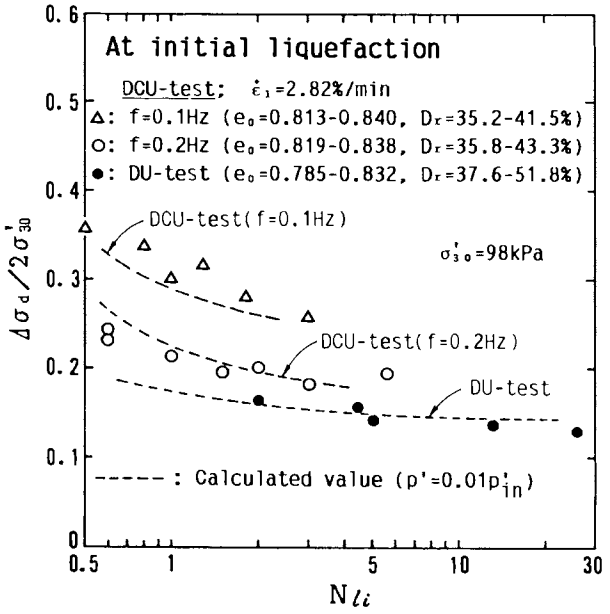

Fig. 14 Prediction of Frequency-Dependency in DCU-test by Proposed Equations

CONCLUSIONS

Cyclic undrained behaviors of saturated sand under DCU-condition was different from those under DU-condition. Because of constant rate static strain, liquefaction strength in DCU-test increased from those in DU-test. And liquefaction strength depended on the frequency of cyclic loading.

The proposed constitutive equations can express the undrained behaviors of saturated sand in DCU-tests, including frequency-dependency of liquefaction strength. These equations are applicable to predict cyclic undrained behaviors of saturated sand for the wide range of stress paths.

ACKNOWLEDGMENTS

The authors wish to appreciate to Mr. S. Sakamoto and Mr. T. Yamada, graduate student of Nagoya university, for their cooperation to dynamic tests.

REFERENCES

Moroto, N. (1976), "A NEW PARAMETER TO MEASURE DEGREE OF SHEAR DEFORMATION OF GRANULAR MATERIAL IN TRIAXIAL COMPRESSION TESTS", Soils and Foundations, 16, 4, 1-9.

Valanis, K. C. (1971), "A theory of visco-plasticity without a yield surface, Part I General theory", Archives of Mechanics, 23, 4, 517-533.